Effects of size distribution on hysteresis losses of magnetic nanoparticles for hyperthermia

2008 J. Phys.: Condens. Matter 20 385214

(http://iopscience.iop.org/0953-8984/20/38/385214)

IOP Publishing Journal of Physics: Condensed Matter

J. Phys.: Condens. Matter **20** (2008) 385214 (12pp) doi:10.1088/0953-8984/20/38/385214

Effects of size distribution on hysteresis losses of magnetic nanoparticles for hyperthermia

Rudolf Hergt[1], **Silvio Dutz**[1] **and Michael Röder**[2]

[1] Institute of Photonic Technology, Albert-Einstein-Strasse 9, 07745 Jena, Germany
[2] Innovent Technologieentwicklung e.V., Pruessingstrasse 27B, 07745 Jena, Germany

E-mail: hergt@ipht-jena.de

Received 5 May 2008, in final form 4 August 2008
Published 27 August 2008
Online at stacks.iop.org/JPhysCM/20/385214

Abstract

For understanding hysteresis losses of magnetic nanoparticles to be used for magnetic particle hyperthermia the effect of size distribution on the dependence of hysteresis losses on magnetic field amplitude is studied on the basis of a phenomenological model in the size range from superparamagnetism to magnetic multi-domains—roughly 10 up to 100 nm. Relying on experimental data for the size dependence of coercivity, an empirical expression for the dependence of hysteresis loss on field amplitude and particle size is derived for hypothetical monodisperse particle ensembles. Considering experimentally observable size distributions, the dependence of loss on distribution parameters—mean particle size and variance—is studied. There, field amplitude is taken into account as an important parameter, which for technical and biomedical reasons in hyperthermia equipment is restricted. Experimental results for different particle types with mean diameter of 30 nm may be well reproduced theoretically if a small loss contribution of Rayleigh type is taken into account. Results show that the Stoner–Wohlfarth model for single domain magnetization reversal via homogeneous rotation cannot explain experimental observations. In particular, in magnetosomes which are distinguished by nearly ideal crystallographic shapes and narrow size distribution large friction-like losses occur even for small field amplitude. Parameters of the high frequency field for hyperthermia (amplitude and frequency) as well as of the size distribution of applied particles are discussed with respect to attaining maximum specific heating power.

(Some figures in this article are in colour only in the electronic version)

1. Introduction

Magnetic particle hyperthermia has been intensively studied as a promising new tumour therapy in recent years (e.g. Moroz *et al* 2002, Gneveckow *et al* 2005, Johannsen *et al* 2007). For temperature enhancement in the tumour by means of magnetic nanoparticles (MNPs) it is desirable to achieve a therapeutic effect with an amount of magnetic material as low as possible. This implies that the heating power generated per particle unit mass should be as high as possible. This is particularly important for applications where target concentration is very low, for instance in antibody targeting of tumours (Hilger *et al* 2005). Magnetic losses, i.e. the amount of magnetic field energy converted into heat during magnetization reversal, are caused by different processes occurring in the particle system: (1) hysteresis, (2) Néel or Brown relaxation, and (3) frictional losses in viscous suspensions. Processes of magnetization reversal in the nanoparticle size range of interest for hyperthermia—roughly 10 up to 100 nm—may vary considerably in dependence on particle size. While magnetic domain wall motion dominates in multidomain particles, with decreasing particle size a transition to homogeneous rotation of the magnetization in single domain particles occurs via different pseudo-single-domain states ('vortex' states; for details see, e.g., Hubert and Schäfer 1998).

Recent experimental investigations have shown that the specific loss power (SLP) of different particle types may vary by orders of magnitude in dependence on structural

and magnetic particle properties as well as magnetic field amplitude (e.g. Hergt *et al* 2006). However, so far it is not clear by what practical means and to what extent it may be possible to enhance SLP. Though SLP is an increasing function of frequency f and field amplitude H in a wide parameter range, the opportunities for enhancement of SLP by an increase of f and/or H are limited. Technical problems increase considerably with increasing frequency when large magnetic field amplitudes are realized in a volume needed for exposure of a human torso. At the same time the costs of therapeutic equipment increase dramatically. Even more importantly, there is a strict limitation of the product Hf for biomedical reasons (see e.g. Brezovich 1988). The alternating magnetic field also causes—in addition to the therapeutically useful heating effect of magnetic particles—an unwanted non-selective heating of both cancerous and healthy tissue due to the generation of eddy currents. To avoid these difficulties the choice of a value of field amplitude far below saturation may be appropriate. In this low amplitude range a typical field dependence of hysteresis loss was observed which shows considerable deviations from current theoretical models (Dutz *et al* 2007b). In particular, the threshold field of the well known model of Stoner and Wohlfarth (1948) for uniform magnetization reversal in single domain particles is not observed in experiment. Instead, a power law for the field dependence of losses is found in the small amplitude regime as demonstrated by the experimental data compiled in figure 1 (Hergt *et al* 2006). Theoretical understanding till now is complicated, since there are several superposing effects influencing SLP, which may not clearly be separated by experiment. Most importantly, it is not possible so far to produce particle ensembles with size distribution sufficiently narrow to show only one defined reversal mechanism. Size distributions of particle suspensions commonly are rather broad (mostly log-normal distributed) and may extend from single domain—or even superparamagnetic—to multidomain size range. Accordingly, the size distribution width is an important parameter, the effect of which on hysteresis loss in nanoparticle systems is not yet clear. Though the effect of size distribution on loss power density in superparamagnetic particle systems was elucidated in the frame of the relaxation theory by Rosensweig (2002), these results are restricted to a narrow size range of superparamagnetic particles due to the limiting suppositions of the underlying linear theory.

Besides particle size, also magnetic properties—in particular anisotropy—of the particle ensemble may be distributed due to varying shape, impurity content or structural imperfections of the particles. A further important issue is clustering of particles which may lead to magnetic interactions, the theoretical description of which meets difficulties. A separation of the different influencing effects would be very valuable for a better understanding of magnetic loss processes in magnetic nanoparticles. The lack of theoretical understanding of current experimental results is not only an obstacle for developing more effective MNP for hyperthermia but also it complicates the prognosis of upper limits for useful SLP, though in a cautious estimation an order of magnitude of 10 kW g^{-1} was given (Hergt and Dutz 2007).

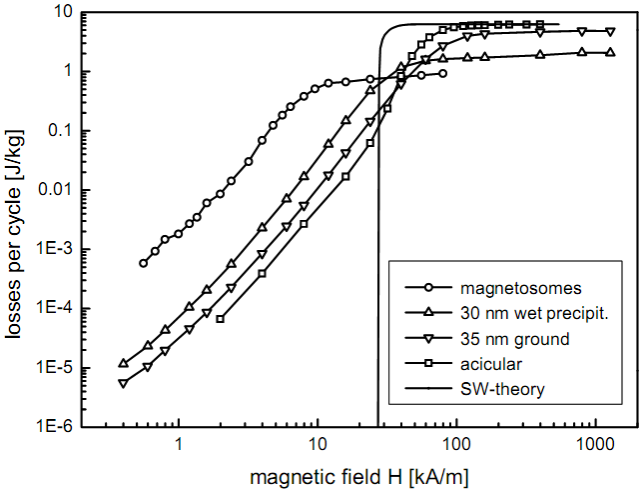

Figure 1. Dependence of magnetic hysteresis loss on the field amplitude of minor loops for the Stoner–Wohlfarth model (full line) in comparison to experimental data of different types of magnetic nanoparticles: wet precipitated, ground, magnetosomes and acicular particles. Reproduced from Hergt *et al* 2006 with permission. Copyright 2006 IOP Publishing Ltd.

Keeping in mind these problems, it is the goal of the present work to elucidate the effect of size distribution on magnetic hysteresis losses in the diameter range from 10 to 100 nm. Considering that different microscopic mechanisms of magnetization reversal are effective in this diameter range and a universal theoretical model does not exist, a phenomenological approach is chosen. First, reasonable analytic expressions for the dependence of losses on particle size and magnetic field are derived. Then, describing the particle size by Γ-distributions, the effect of the distribution parameters on magnetic losses of the particle ensemble is calculated. As a result, guidelines for the choice of mean particle size are derived for practical cases when size distribution is large and/or magnetic field amplitude is restricted to low values below saturation.

2. Basic assumptions

In general, losses in magnetic materials may be determined experimentally by measuring hysteresis loops (see, e.g., Bertotti 1998). While the dependence of hysteresis loss on field amplitude may differ considerably for different materials, a common feature is an increase of loss with increasing loop amplitude until a saturation value is reached. For studying the effect of particle size distribution on hysteresis loss one has to know—either by experiment or from theory—the field dependence of losses for so-called 'monodisperse' particle ensembles. Unfortunately, monodisperse particles are not available in the currently interesting size range. Moreover, a universal theory of the field dependence of losses does not exist. In the special case of an ensemble of statistically oriented, monodisperse, ellipsoidal, uniaxial, single domain particles the Stoner–Wohlfarth model predicts magnetization reversal by the uniform mode, so-called homogeneous rotation. In this case, the hysteresis loss is proportional to the product

of coercivity and remanence. Recently, by experimental investigations of different types of maghemite (γ-Fe_2O_3) and magnetite (Fe_3O_4) nanoparticles in the transition range between single and multidomain behaviour, it was shown that hysteresis loss is generally proportional to coercivity (Dutz *et al* 2007b). Considering that a theory of hysteresis loss for the interesting wide size range does not exist, the empirical approach used in the following relies on the experimentally justified assumption that the main parameter describing hysteresis loss is coercivity. Accordingly, in the following reasonable assumptions on firstly the size dependence of coercivity and secondly the field dependence of losses are derived.

2.1. Size dependence of coercivity

The size dependence of coercivity was investigated in the literature for different magnetic materials. Experimental results for specific substances as well as schematic drawings of the general shape of the size dependence of coercivity may be found in several textbooks (e.g. Kneller 1966, 1969, Kronmüller and Fähnle 2003). For multidomain particles of magnetite, comprehensive experimental data were reported by Heider *et al* (1987), which show a power law increase of loss with decreasing size in a wide size range from some micrometres down to 30 nm. Similar power laws were found for other substances, as described in the monograph of Kneller (1966, 1969). As a basis of the following calculations the power law reported by Heider *et al* is adopted for describing the coercivity in the multidomain size range

$$H_c^{md}(D) = H_M(D/D_1)^{-0.6} \quad (1)$$

(H_M and D_1 are empirical parameters to be specified below).

With decreasing particle size, domain walls become energetically unfavourable and a transition to single domain particles occurs. Coercivity is determined by anisotropy contributions due to crystal structure, particle shape and surface. In the simplest case of uniaxial anisotropy, for an ensemble of non-interacting, ellipsoidal single domain particles the model of Stoner and Wohlfarth (1948) predicts magnetization reversal by homogeneous rotation. For this uniform mode, hysteresis loss energy density for randomly distributed particle axes is given by twice the anisotropy energy density K; coercivity is half of the anisotropy field $H_A = 2K/\mu_0 M$ (M magnetization). The dependence of hysteresis loss on field amplitude for randomly oriented particles is shown in figure 1.

In comparison with the case of uniaxial particles the situation is more complex for cubic anisotropy. Kneller (1966, 1969) has given $H_c = 0.64\ K/\mu_0 M$ for $K > 0$ and $0.39\ K/\mu_0 M$ for $K < 0$. The latter is the case for maghemite with $K = -4.6$ kJ m^{-3} and magnetite with $K = -11$ kJ m^{-3} (e.g. Mee and Daniel 1996). However, these small values of crystal anisotropy may be exceeded by shape anisotropy even for relatively small deviations from sphericity. For instance, an elongation with an aspect ratio 1.4 results in a shape anisotropy energy of 20 kJ m^{-3} for magnetite. As a consequence, for a moderate aspect ratio up to 1.4, theoretical values of coercivity may vary from about 4.0 to 25 kA m^{-1} for maghemite and 7.2 to 33 kA m^{-1} for magnetite. Experimental values of coercivity vary essentially in dependence on particle structure. In the case of magnetite, for instance, Heider *et al* (1987) have shown that the coercivity of crushed particles may be larger than that of as-grown ones by a factor which increases from two up to ten with increasing particle size. This is also reflected by the hysteresis loss data shown in figure 1. The saturation loss (and coercivity, cf. (Dutz *et al* 2007b)) of ground particles is roughly twice the value of chemically grown particles. It is well known that particles for recording applications are trimmed to maximum coercivity by several technological means, e.g. acicular shape or Co doping of maghemite. By these means coercivity may be increased to values above 70 kA m^{-1} (Eagle and Mallinson 1967). A typical sample of acicular particles is included in figure 1, too. In contrast, magnetic nanoparticles for the present biomedical applications are grown mainly by different chemical precipitation techniques resulting in nearly equant particle shapes (e.g. Tartaj *et al* 2003).

In figure 2 examples of typical particles of maghemite in the single domain size range are shown. The particles of figure 2(a) exhibit polyhedral shapes. The occasionally appearing combinations of octahedral and cubic faces, which are faces of low specific surface energy of the spinel lattice, indicate that growth occurred near to equilibrium. Nevertheless, irregular shapes occur and particle size varies considerably. In contrast, particles shown in figure 2(b), being wet chemically precipitated too, have a spherical appearance with a berry-like substructure, presumably due to growth under conditions of higher supersaturation. The 'berries' consist of several single crystals of about 15 nm mean diameter, the crystal lattices of which are incoherent according to XRD measurements. Magnetosomes shown in figure 2(c), which are synthesized by magnetotactic bacteria (see, e.g., Heyen and Schüler 2003), represent a special case. They are characterized by regular polyhedral shape and narrow size distribution. Magnetic properties of these 'naturally' synthesized particles differ remarkably from artificially grown ones (cf figure 1). They have delivered the till now largest values of specific loss power (Hergt *et al* 2005). In addition, figure 2(d) shows commercial maghemite having nearly spherical particles and a very broad size distribution, which is shown below in figure 5(b). Particles of similar spherical habit were also prepared by laser vapour condensation (Kurland *et al* 2007).

While for ellipsoidal particles magnetization curling is assumed theoretically to be the preferred reversal mode (Aharoni 1996), it was found experimentally that particles deviating strongly from ellipsoids meet difficulties with theoretical explanation. For very elongated (rod shaped) particles complicated modes of magnetization reversal (e.g. buckling, fanning) were predicted by theory. For real particles, the role of imperfections for the nucleation problem as well as the presence of corners at polyhedra where the demagnetizing field diverges are controversially discussed in the literature (see, e.g., Aharoni 1997). Micromagnetic calculations for cubic particles using finite difference methods (e.g. Kronmüller and Fähnle 2003) reveal sophisticated magnetization patterns like the so-called flower and vortex

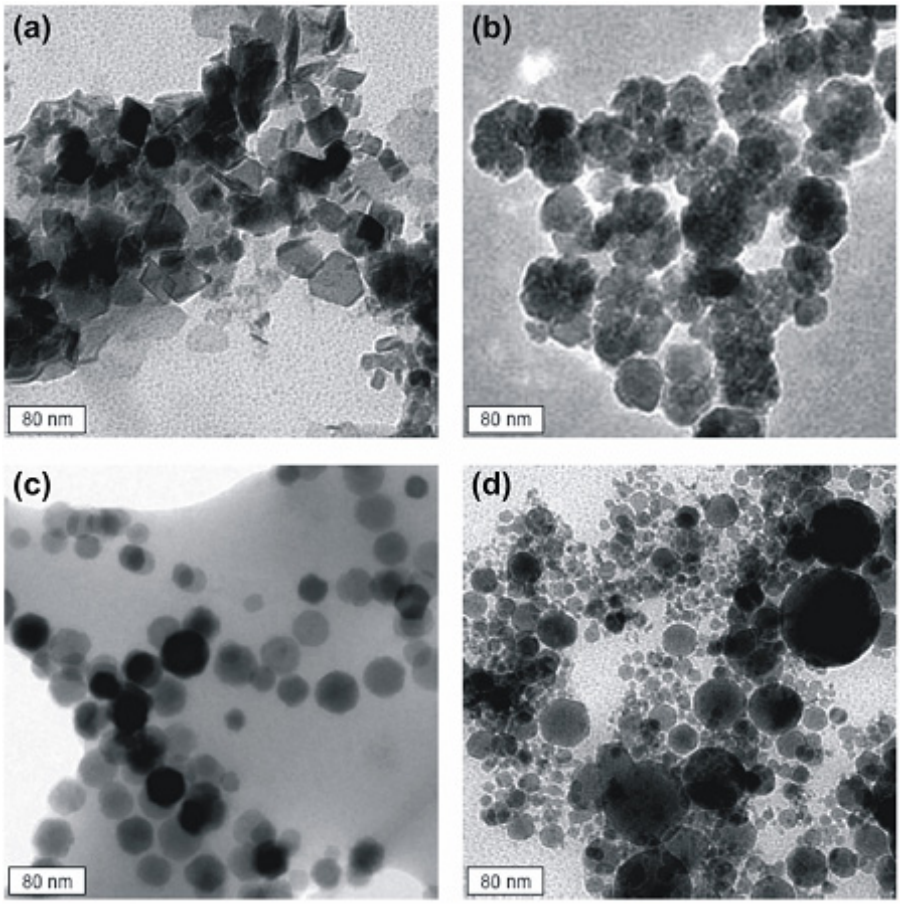

Figure 2. Examples of different types of magnetic nanoparticles with a mean diameter of about 30 nm: (a) wet precipitated polyhedra (Dutz *et al* 2005), (b) wet precipitated 'berries' (Dutz *et al* 2007a), (c) magnetosomes, and (d) commercially available spheres (iron(III) oxide, gamma, 99+%, AlfaAesar, Karlsruhe, Germany).

states (Fabian *et al* 1996) in the transition range from single to multidomain. Improved calculations of Witt *et al* (2005) for octahedral particles show a transition from flower to vortex states above about 80 nm (spherical diameter), in fair accordance with earlier predictions for tetragonal particles of Butler and Banerjee (1975).

When particle size is decreasing the barriers for magnetization reversal come into the order of magnitude of thermal energy and so-called superparamagnetic fluctuation effects result. These relaxation effects cause vanishing of remanence and coercivity as well as hysteresis losses if the characteristic time of measurement τ_m is larger than the relaxation time τ_R of the particle system. The latter is determined for immobilized particles by the ratio of the anisotropy energy KV (V is mean particle volume) to the thermal energy kT (Néel 1949)

$$\tau_R = \tau_0 \exp[KV/(kT)] \qquad (\tau_0 \sim 10^{-9}\ \mathrm{s}). \tag{2}$$

This very strong size dependence of the relaxation time causes a steep decrease of coercivity in the superparamagnetic regime, which is experimentally well documented (see, e.g., Kneller 1966, 1969). Experimental observations may be approximated by

$$H_c^{sp}(D) = H_M[1 - \exp(-D/D_1)^5] \tag{3}$$

with the same parameters as in equation (1). Combining equations (1) and (3), one gets the expression

$$H_c(D) = H_M(D/D_1)^{-0.6}[1 - \exp(-D/D_1)^5]. \tag{4}$$

There are two parameters, H_M [kA m^{-1}] and D_1 (nm), which may be used to reproduce experimental data of particular magnetic materials. For instance, for wet chemically grown magnetite $H_M = 32$ kA m^{-1} and $D_1 = 15$ nm seem to be an appropriate choice. For these parameters equation (4) is shown in figure 3. It covers the regions of different types of magnetization reversal discussed above. For comparison, experimental data points taken from the work of Heider *et al* (1987) are shown, too. The maximum coercivity of 26 kA m^{-1} at a particle size of about 19 nm is in accordance with experimental observations. In the following, equation (4) is considered as a representative approximation for empirical data of the size dependence of coercivity in the complete size interval from superparamagnetism up to the multidomain size range.

2.2. Dependence of specific magnetic losses on field amplitude

For the simple case of homogeneous magnetization reversal in ellipsoidal, uniaxial magnetic particles the well known Stoner–Wohlfarth (SW) model (Stoner and Wohlfarth 1948) predicts

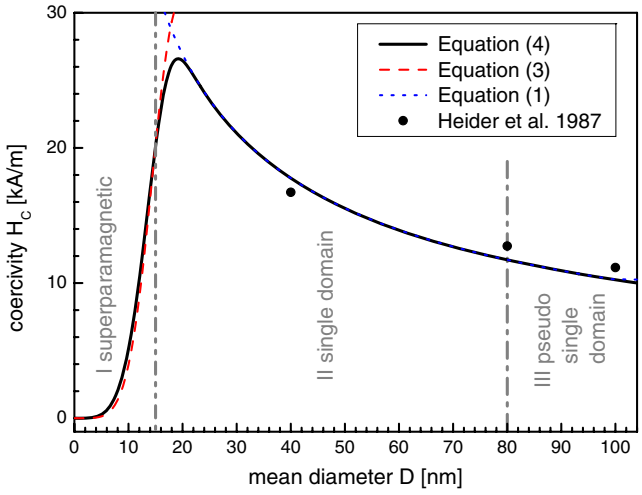

Figure 3. Dependence of coercivity on particle diameter assumed for the present calculations (cf text).

for the onset of hysteresis losses a threshold field $H_c = H_A/2$, below which loss is zero. Above the anisotropy field H_A one attains the saturation loss $4B_R H_c$ (B_R is remanent flux density), which was found experimentally to be proportional to coercivity (Dutz *et al* 2007b, Müller *et al* 2006). Accordingly, for monodisperse single domain particles the dependence of specific hysteresis loss w_{sw} on the field amplitude H of minor hysteresis loops is approximated by

$$w_{sw}(H) = \begin{cases} 0 & \text{for } H \leqslant H_c \\ \dfrac{4B_R H_c}{\rho}\left(1 - \left(\dfrac{H_c}{H}\right)^5\right) & \text{for } H > H_c \end{cases} \qquad (5)$$

where ρ is the mass density of the magnetic material (4800 kg m^{-3} for maghemite).

The specific loss power (SLP, measured in watts per gram of magnetic material) which is converted into heat in an external high frequency field is given by multiplying specific hysteresis loss energy by the frequency f of the exciting field according to

$$\mathrm{SLP}(H, f) = w_{sw}(H) f. \qquad (5a)$$

Below the single domain size range superparamagnetic fluctuations cause the measured hysteresis losses to decline rapidly with decreasing particle size. In a small amplitude approximation, i.e. in a linear regime, the specific loss power (SLP) of superparamagnetic particles (occasionally termed 'relaxation losses') may be expressed in terms of the imaginary part $\chi''(f)$ of the susceptibility according to (see, e.g., Landau and Lifshitz 1960)

$$\mathrm{SLP}(H, f) = \mu_0 \pi \chi''(f) H^2 f/\rho. \qquad (6)$$

The spectrum of $\chi''(f)$ shows a peak situated at the reciprocal of the relaxation time τ_R (Debye 1929):

$$\chi''(f) = \chi_0 \phi(f)/(1 + \phi(f)^2), \qquad \phi(f) = f\tau_R, \qquad \chi_0 = \mu_0 M_S^2 V/(kT) \qquad (7)$$

where M_S is the saturation magnetization.

The very strong size dependence of the relaxation time according to equation (2) causes a sharp maximum of SLP in dependence on particle size. Accordingly, a remarkable output of heating power occurs only for particle systems with appropriate 'resonant' size and narrow size (and anisotropy) distribution (Hergt *et al* 1998, 2002). In a relatively small diameter range losses decrease steeply with decreasing size (see, e.g., Hergt and Andrä 2007). For particle size larger than the 'resonant' one the linear description of relaxation theory ceases and hysteresis loss has to be described by equation (5), which will be used in the following.

For taking into account the superparamagnetic decline of coercivity—and consequently hysteresis loss—the size dependence of the coercivity given by equation (4) is introduced into equation (5). For representing experimentally observed saturation loss $B_R = 0.1$ is chosen. The resulting loss 'landscape' $w_{sw}(H, D)$ for SW-like monodisperse particles is shown in figure 4(a). The saturation 'plateau' is smoothly

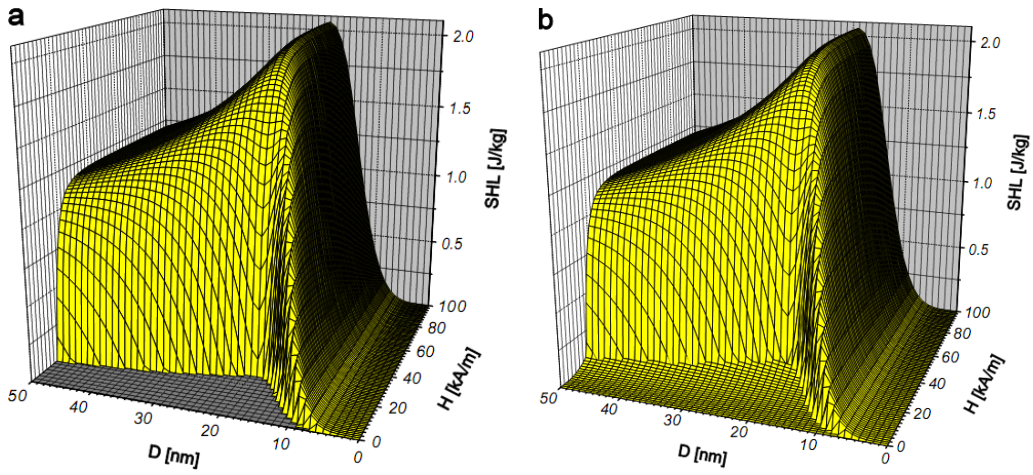

Figure 4. Dependence of magnetic losses on particle diameter and magnetic field amplitude for the Stoner–Wohlfarth model (a) and the same with additional consideration of a loss contribution of Rayleigh type (b).

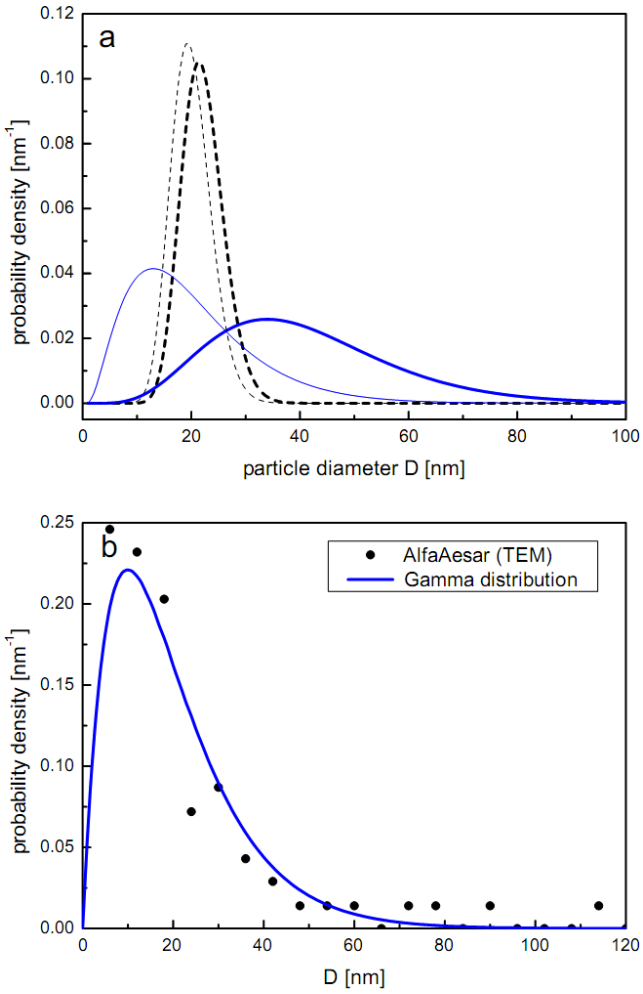

Figure 5. (a) Typical examples of a narrow ($D_0 = 0.7$ nm, dashed lines) and a broad ($D_0 = 7$ nm, full lines) particle size distribution used in the present calculations. Number weighted (fine lines) as well as volume weighted (bold lines) distributions are shown. (b) An experimentally found very broad distribution of commercial maghemite particles.

declined towards larger size and is bounded by a steep 'cliff', which emerges from a 'coastline' given by the function $H_c(D)$.

As mentioned above, in real particle ensembles a threshold field is not observed. In figure 1 the prediction of the SW model is compared with experimental data of magnetic particle types prepared in quite different ways (wet chemical precipitation, grinding, bacterial synthesis, acicular material from the recording industry) of nearly equal mean particle size of the order of 30 nm for the equi-axial materials. The acicular particles have typical dimensions of about 30 nm diameter and 300 nm length. For all the differently prepared particles the functional dependence $w(H)$ is similar but deviates principally from the SW model. Instead of a threshold field, experimentally a power law is found at low field amplitudes. One may guess that this power law is caused by a broad size distribution resulting in the presence of particles having different coercivities. However, if the size distribution extends into the multidomain size range one has to consider a contribution of Rayleigh losses, too. Those losses caused by pinning of magnetic domain walls may be described by a third order power law for small amplitudes (see, e.g., Kronmüller and Fähnle 2003).

$$w_R \sim H^3. \tag{8}$$

Consequently, in order to take into account losses of Rayleigh type one has to provide a corresponding correction term in equation (5), which in the present calculations is chosen according to

$$w(H, D) = \begin{cases} \alpha D H^3 & \text{for } H \leqslant H_c \\ \dfrac{4 B_R H_c(D)}{\rho} \cdot \left(1 - \left(\dfrac{H_c(D)}{H}\right)^5\right) & \text{for } H > H_c \end{cases} \tag{9}$$

where the parameter α is a measure of the Rayleigh type loss contribution. The resulting shape of the loss face $w(H, D)$ with $\alpha = 4 \times 10^{-7}$ J m^2 kg^{-1} A^{-3} is shown in figure 4(b). At the foot of the steep cliff of figure 4(a) now a shallow shelf occurs.

2.3. Size distribution of the nanoparticle ensemble

It is well known from the literature that most methods for magnetic nanoparticle preparation result in log-normal size distributions. This is valid, in particular, for the widely used wet chemical precipitation methods.

In order to find the effect of a particle size distribution, the hysteresis losses given by equations (5) and (9) have to be weighted with the particle size distribution $f(D)$ according to

$$W(H) = \int w(H, D) f(D)\, \mathrm{d}D. \tag{10}$$

For weighting the loss energy with the particle size correctly one has, of course, to use the volume weighted distribution. It is calculated from the number weighted distribution $f_n(d)$, which often is determined from imaging (e.g. TEM) of the particle ensemble according to

$$f(D) = \frac{\pi f_n(D) D^3}{6V}, \qquad V = \frac{\pi}{6} \int f_n(D) D^3\, \mathrm{d}D. \tag{11}$$

For mathematical description of the magnetic particle size distribution we use instead of the currently used log-normal distribution the Γ-distribution (see e.g. Aharoni 1996) which is equivalent in shape but has advantages with the numerical calculation of the integrals, which was performed in the present case with the software MATHCAD®

$$f_n(D) = \frac{1}{D_0} \left(\frac{D}{D_0}\right)^{\beta} \mathrm{e}^{\left(-\frac{D}{D_0}\right)} \frac{1}{\Gamma(\beta + 1)} \qquad \beta = \frac{m}{D_0} - 1 \tag{12}$$

where m is the mean size. The variance is given by $(m D_0)^{1/2}$.

Figure 5(a) shows two examples of number and corresponding volume weighted size distributions taken for the calculations given below to be representative for a 'monodisperse' and an actually observed broadly distributed particle ensemble. The parameters of the corresponding

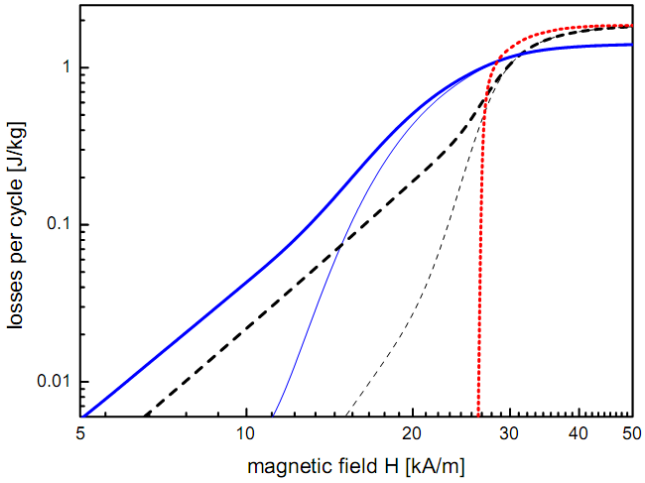

Figure 6. Dependence of magnetic losses on magnetic field amplitude for narrow ($D_0 = 0.7$, dashed lines) and broad ($D_0 = 7$, full lines) size distribution both with (bold lines) and without (fine lines) consideration of a loss component of Rayleigh type. The dotted line represents Stoner–Wohlfarth theory.

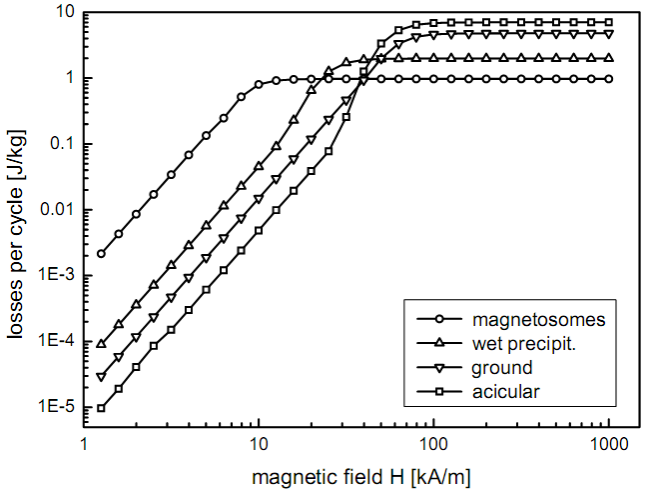

Figure 7. Experimental curves of figure 1 reproduced by model calculations taking into account particle size distribution.

number weighted distribution are mean size $m = 19$ nm for both distributions and $D_0 = 0.7$ and 7 nm for the 'monodisperse' and for the broad distribution, respectively. As an example for experimentally observed size distributions, in figure 5(b) the measured size distribution of a commercial maghemite powder (iron(III) oxide, gamma, 99 + %, AlfaAesar, Karlsruhe), the particles of which are shown in figure 2(d), is given. Parameters of the Γ-distribution fitted to experimental data points are $m = 20$ and $D_0 = 10$ nm. This distribution was determined by means of transmission electron microscopy as well as atomic force microscopy. By x-ray diffraction a mean particle size of 30 nm was derived from line width according to the Scherrer formula.

3. Hysteresis loss of nanoparticle ensembles

The magnetic hysteresis loss of a nanoparticle system is given by equation (10) as a function of the field amplitude of the hysteresis cycle. In practice, the field amplitude is mainly determined by technical and medical conditions of the hyperthermia therapy equipment. The dependence of hysteresis loss on field amplitude for a narrow and a broad size distribution as well as the influence of an eventually arising loss contribution of the Rayleigh type will be discussed in section 3.1. In addition, the effect of the two parameters of the particle size distribution—mean particle diameter and diameter variance—occurring in equation (10) will be discussed in section 3.2. In section 3.3 the question of the maximum hysteresis loss under an additional biomedical constraint will be discussed.

3.1. Dependence of hysteresis loss on magnetic field amplitude

The dependence of hysteresis loss of a nanoparticle ensemble on the field amplitude of hysteresis minor loops calculated according to equation (10) is shown in figure 6 for a quasi-monodisperse (dashed lines, $D_0 = 0.7$ nm) and a rather broad, usually found size spectrum (full lines, $D_0 = 7$ nm). The mean diameters of the number distributions were chosen identically, $m = 19$ nm, corresponding to the maximum coercivity of the single domain state (cf figure 3). In addition, in figure 6 the influence of a minor contribution due to Rayleigh type losses is demonstrated. Curves symbolized by fine lines are calculated using the 'Stoner–Wohlfarth-' (SW-) like equation (5), while for the pair of bold lines Rayleigh type losses were taken into account according to equation (9). For comparison, the curve of the exact SW theory is shown, too. The curves calculated according to equation (5) by taking into account a size distribution of the magnetic particles show deviations from SW at small amplitudes, which are the more obvious the broader the distribution is. However, comparison with experimental curves presented in figure 1 shows that even the broader distribution cannot explain the experimental data. A satisfying reproduction of shapes for the experimental curves may be attained only by taking into account a contribution of losses of Rayleigh type, e.g. due to a small fraction of multidomain particles. The corresponding bold lines in figure 6 reproduce the experimentally observed third order power law, though the assumed portion of wall pinning is comparatively small. The results show that the occurrence of a third order power law in the field dependence of hysteresis losses may be interpreted as an experimental indication for the presence of a small portion of multidomain particles, even if imaging results (e.g. by TEM) indicate a small mean particle size in the single domain range.

The model calculations, examples of which are shown in figure 6, also explain the experimentally observed 'crossover' of curves (Dutz *et al* 2007b): above the coercivity field narrow distributions give larger hysteresis loss while for field amplitudes below coercivity broader distributions are superior with respect to losses. The usefulness of the empirical model is demonstrated in figure 7, where the experimental curves of figure 1 were reproduced by model calculations

Table 1. Parameters used for simulation of the curves shown in figure 7.

Particle type	m (nm)	D_0 (nm)	H_M (kA m^{-1})	B_R (T)	$\alpha[10^{-7}]$ (J m^2 kg^{-1} A^{-3})
Magnetosomes	30	2	11	0.175	300
Wet precipitated	30	5	35	0.125	10
Ground	35	5	90	0.125	3
Acicular	30	6	80	0.200	1

using reasonable physical parameters. These parameters are compiled in table 1. While the mean diameter of the different particle types is nearly the same, the different amplitude dependences of the samples may be well understood by reasonable differences of the other parameters given in table 1. For instance, the magnetosome particles are characterized by a uniform size (cf figure 2(c)) and a crystallographically well defined shape, which makes reasonable the low value of $D_0 = 2$ nm as well as the small $H_M = 11$ kA m^{-1}, the latter being of the order of the crystal anisotropy field. Large values of H_M result for the magnetically hard acicular and ground particles, while wet precipitated particles have a moderate $H_M = 35$ kA m^{-1}. These data as well as the relatively low values of B_R of the order of $0.1 \cdots 0.2$ T, which are smaller than predictions of the SW model, are in accordance with experimental results discussed above (Heider *et al* 1987, Dutz *et al* 2007b). It should be pointed out that the remanence of a particle ensemble may essentially be influenced by magnetic particle interactions, which, however, are beyond the scope of the present paper. Remarkably large variations occur for the parameter α. It increases strongly from low values for magnetically hard particles via the relatively soft wet precipitated ones to an extremely large value for magnetosome particles. This is a clear indication that in these particles the magnetization reversal is accompanied by friction-like loss processes rather than by SW-type instabilities, though magnetosome particles with a mean diameter of 30 nm and a small variance of 8 nm are clearly in a size range commonly considered to be typical for the uniform SW-reversal mode of single domain particles. Though α was introduced above in relation to Rayleigh losses, it is clear that classical domain walls may not be expected in magnetosome particles. Magnetization structures in these particles were calculated by Witt *et al* (2005), applying an improved numerical method for a realistic crystallographic model of magnetosome particles. It was found that a transition from flower state to vortex state may occur in large magnetosomes. For octahedral particles these authors found that there exists an extremely broad metastable range between about 80 and 300 nm where particles may support flower as well as vortex states.

Though magnetization dynamics has not been investigated till now, one may imagine that a transition involving these complicated non-uniform magnetization patterns is accompanied by considerable losses. Field induced changes of the local tilt of spins which are canted with respect to the crystal lattice as well as to each other may result in friction-like dissipation due to spin–lattice interactions in these inhomogeneous structures. It is this relatively high loss in the low field amplitude range which makes magnetosome particles interesting for magnetic heating (cf Hergt *et al* 2005). However, considering the chain-like structures of magnetosomes, one may expect that their magnetic behaviour is at least partially determined by interactions, too. Dunin-Borkowski *et al* (2001) have shown by electron holography of magnetotactic bacteria that single particles are aligned with magnetic easy [111] axes parallel to the chain axis. The fanning reversal mechanism may apply as far as chains are intact. Wet precipitated particles shown in figure 2(b) are also magnetically soft and exhibit fairly large losses at small field amplitude. The magnetization structure in these particles may be even more complicated than in magnetosomes. Due to the 'berry'-like structure, weakly coupled regions may exist, which may result in a relatively low remanence, while magnetization changes occur with considerable energy dissipation.

3.2. Dependence on size distribution parameters

If technical parameters for hyperthermia equipment—mainly field amplitude and frequency—are fixed, the question for the optimum relation of particle properties and field amplitude holds. For evaluation of the effect of a particle size distribution, a variation of the distribution parameters m and D_0 with respect to hysteresis losses was performed. Figure 8 shows the dependence of hysteresis loss on mean particle size m for a narrow (figure 8(a), $D_0 = 0.7$) and a broad (figure 8(b), $D_0 = 7$) size distribution for different values of the hysteresis loop amplitude. In both cases a loss contribution of Rayleigh type was taken into account. Of course, a reduction of field amplitude below saturation results in a decrease of heat output. However, the curves show clearly that the amount of decrease depends specifically on the mean size and the distribution width. Reasonably, the broad distribution is not very sensitive to a change of mean size. In contrast, the narrow distribution shows a marked depression of losses for medium mean sizes. This minimum of hysteresis loss is the more pronounced the lower the field amplitude is. Clearly, the reason is that in a narrow distribution a relatively large portion of particles may be present, the coercivity of which is larger than the hysteresis loop amplitude. The maximum loss may be gained only if field amplitude is above the coercivity of the majority of particles. As a consequence, if the field amplitude is limited to a value below saturation—e.g. for technical reasons—a broader size distribution may be favourable to get large heat output for hyperthermia. The effect of a Rayleigh type loss contribution is shown in figure 8(c) for a narrow and a broad distribution.

The optimum mean particle size derived from the maxima of curves of the type shown in figures 8(a) and (b) is plotted in figure 8(d) in dependence on the applied field amplitude. Of course, large amplitude and small mean size yield highest hysteresis loss. But, the smaller the amplitudes available for therapy is, the larger the mean particle size that should be chosen for achieving a sufficient heating effect. This tendency is more pronounced for broader distributions.

The dependence of hysteresis loss on size distribution width for a mean size of 19 nm (full lines) and 30 nm (dashed

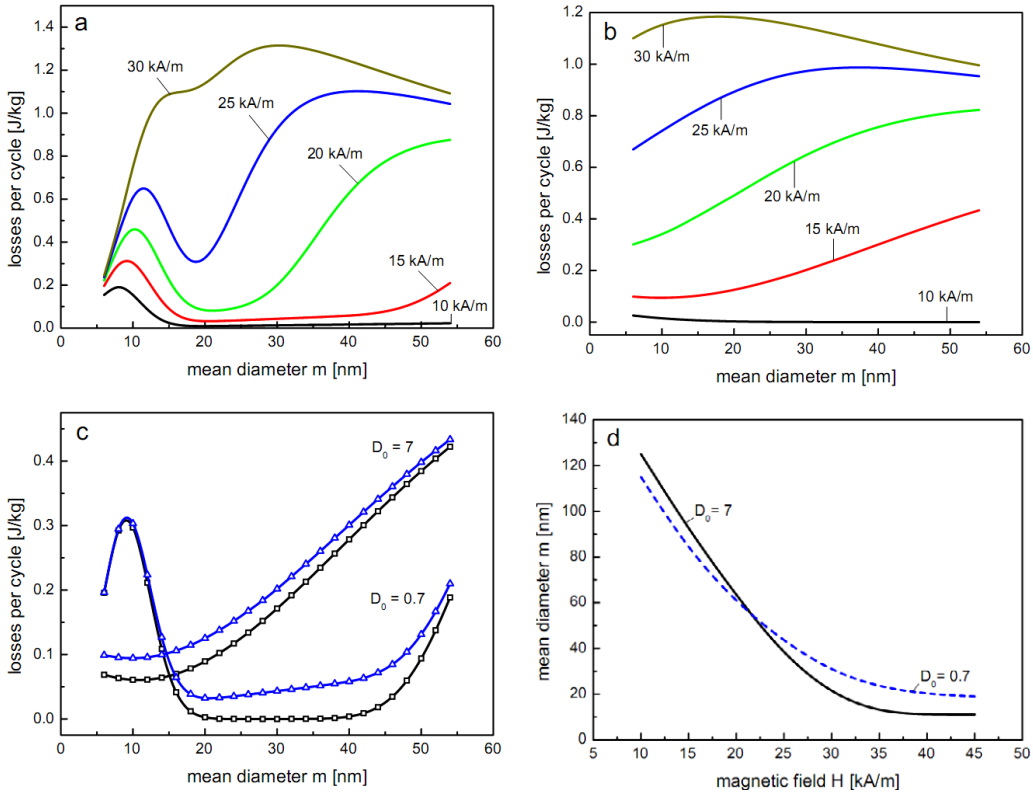

Figure 8. Dependence of magnetic losses on the mean particle diameter for narrow (a) ($D_0 = 0.7$ nm) and broad (b) ($D_0 = 7$ nm) size distributions with consideration of a loss component of Rayleigh type for different magnetic field amplitudes (10, 15, 20, 25, 30 kA m^{-1}). The contribution of Rayleigh-like losses (triangles) for a narrow ($D_0 = 0.7$ nm) and a broad ($D_0 = 7$ nm) size distribution is shown in (c) for a field amplitude of 15 kA m^{-1}. Optimum pairing of field amplitude and mean size is shown in (d).

lines) is shown in figure 9 for three different field amplitudes. Again, a remarkable dependence of hysteresis loss on size distribution parameters is observed for field amplitudes lower than the coercivity field. While for a field amplitude near saturation (35 kA m^{-1}) there is a relatively weak dependence on distribution width as well as mean diameter, for a small field amplitude of 15 kA m^{-1} broader distributions are clearly favourable with respect to hysteresis loss for both values of mean size. Highest loss occurs for the smaller mean size with small distribution width only near saturation. For lower amplitudes the larger mean size of 30 nm combined with the broader distribution is favourable for high loss.

3.3. Optimization of magnetic nanoparticles for hyperthermia

As already mentioned above, there are several factors which forbid an enhancement of the heating power of magnetic particles by simply increasing field amplitude and/or frequency. In particular, a non-selective tissue heating due to eddy currents has to be avoided in magnetic particle hyperthermia. According to the induction law the eddy current power is proportional to the square of (Hfd), where d is the induced current loop diameter. Considering the specific electrical conductivity of tissue (0.6 Ω^{-1} m^{-1}), the critical current density for irreversible cell damage (of the order of 20 mA cm^{-2}, see, e.g., Siegenthaler 1994) may be reached in macroscopic loops of the patients body if the product Hf exceeds a critical value C.

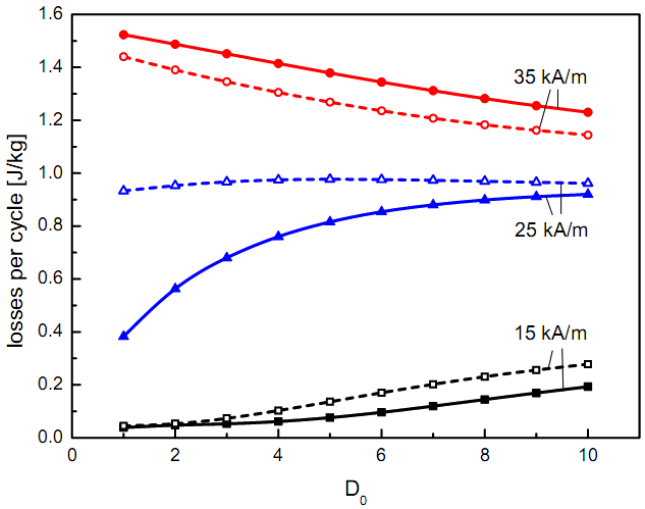

Figure 9. Dependence of magnetic losses on size distribution width for different mean particle diameters (19 nm, full lines, and 30 nm, dashed lines) for field amplitudes of 15, 25 and 35 kA m^{-1}.

For instance, for the first commercially developed equipment for treatment of human patients the frequency and field amplitude are limited to 100 kHz and 18 kA m^{-1}, respectively (Gneveckow *et al* 2004). Brezovich (1988) has found in experiments with volunteers for a loop diameter of

about 30 cm that a '*test person had a sensation of warmth, but was able to withstand the treatment for more than one hour without major discomfort*' if $Hf < 4.85 \times 10^8$ A m^{-1} s^{-1}. For a smaller diameter of the exposed body region and in dependence on the seriousness of the illness this critical product may be exceeded. In the following estimations we assume a rather weak criterion, $C = 5 \times 10^9$ A m^{-1} s^{-1}. By replacing f according to the condition $f(H) = C/H$ in the dependence SLP(f, H) of the relevant loss processes (equations (5*a*) or (6)) one get the optimum combination of f and H for maximum SLP (Hergt and Dutz 2007). Results of applying this procedure to the curves shown in figure 6 (only curves including Rayleigh type losses are considered) are presented in figure 10 for nanoparticle systems with narrow ($D_0 = 0.7$ nm, dashed line) and broad size distributions ($D_0 = 7$ nm, full line). Remarkably, under the Hf-restriction the maximum hysteresis loss power (about 200 W g^{-1}) occurs considerably below saturation. Optimum field parameters are 29 kA m^{-1} at 167 kHz for the broad ($D_0 = 7$ nm) and 36 kA m^{-1} at 139 kHz for the narrow size distribution ($D_0 = 0.7$ nm). Though the broader size distribution has smaller hysteresis loss at saturation field than the narrow distribution (cf figure 6) under the eddy current restriction it may deliver nearly the same loss power as the narrow distribution even for considerably smaller field amplitude. The reason is that the linear increase of saturation hysteresis loss with coercivity cannot be utilized for heating power in hyperthermia due to the just discussed restriction.

It was shown previously (Hergt and Dutz 2007) that under the eddy current restriction single domain magnetosome chains show similar loss power as attained by magnetically hard acicular particles at much larger field. The largest loss power is shown by the theoretical curve of figure 10 for hypothetical SW particles having a larger maximum of hysteresis loss at optimum field parameters than the narrow size distribution which is assumed to have the same saturation loss. However, considering magnetic properties of various particle types in the single domain size range (region II in figure 3)—typical examples of which are shown in figure 2, the hope for future particles which approach the prognosis of the SW model is restricted. At present, best chances for extreme loss power offer experimental results with magnetosomes as discussed above. While commonly available iron oxide ferrofluids show an SLP below about 100 W g^{-1}, in a few special cases experimental values in excess of 500 W g^{-1} up to about 1000 W g^{-1} were found for magnetosomes (Hergt *et al* 2005).

In the superparamagnetic size range SLP(H, f) for relaxation losses (of Néel or Brown type) is given by equations (6) and (7). Introducing here the condition $f(H) = C/H$ one gets the result that with increasing H (and correspondingly decreasing f) one approaches asymptotically the maximum SLP according to (Hergt and Dutz 2007)

$$\mathrm{SLP}_{\max} = (4/5)\mu_0 \pi C^2 \chi_0 \tau_\mathrm{R}/\rho. \qquad (13)$$

As a result, SLP increases in the superparamagnetic regime with increasing relaxation time τ_R (i.e. with increasing particle size) until the validity of the relaxation theory ceases near the transition to the stable single domain regime (Hergt *et al* 1998).

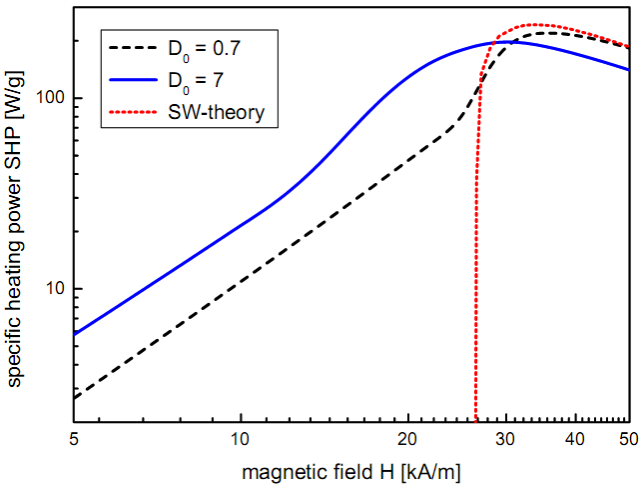

Figure 10. Specific heating power of curves with Rayleigh type losses presented in figure 6 under the additional constraint of an eddy current restriction (cf text).

Experimentally, the validity of the relaxation model was shown for maghemite ferrofluids with a mean particle diameter of 15 nm, which may deliver up to 600 W g^{-1} measured calorimetrically under the condition $C = 5 \times 10^9$ A m^{-1} s^{-1} (Hergt *et al* 2004a, 2004b). For evaluation of experimental results one has to keep in mind that extrapolation from hysteresis loss per cycle to SLP leads to an underestimation as shown for magnetosomes by Hergt *et al* (2005) by comparison with calorimetrical measurements of SLP performed at field parameters to be used for hyperthermia.

4. Conclusions

Summarizing the above results, a useful choice of field amplitude and frequency depends strongly on the parameters of the size distribution of the nanoparticles to be used for hyperthermia. The results show opportunities for enhancement of SLP of magnetic iron oxide nanoparticles: maximum SLP may be expected by preparation of particle suspensions with narrow size distribution and with a mean diameter that corresponds to the maximum coercivity in the single domain size range. In the literature, several attempts were reported to achieve a better controlling of the phase formation processes in order to grow particles with narrow size distribution (see, e.g., Sun and Zeng 2002, Klokkenburg *et al* 2004). One strategy is the separation of the nucleus formation stage from the further particle growth without new nucleation (see, e.g., Müller *et al* 2006). Clustering due to particle interaction has to be avoided by coating particles as soon as possible after finishing the growth process. After growth, size distribution may be further narrowed by magnetic fractionation (Glöckl *et al* 2006). For larger particle sizes sedimentation fractionation may be applied (Dutz *et al* 2008). By this method large clusters may also be eliminated. Though the demand for sedimentation stability is not critical for hyperthermia, a reliable re-dispersion of the sediment must be possible. The above results show that a narrow size distribution needs a good adjustment of mean particle size in relation to the magnetic field amplitude for attaining maximum SLP. In the optimum case field amplitude

is large enough to exceed the coercivity of the majority of particles. If this relation is not obeyed, e.g. due to lack of knowledge of the accurate mean particle size and the corresponding coercivity, many particles cannot reach their maximum SLP. Then, unexpectedly it may be advantageous to use particles with a broader size distribution.

As pointed out above, the effect of size distribution of the particle ensemble investigated in the present paper is only one of several important factors influencing SLP. Another till now insufficiently understood issue is magnetic particle interaction (see, e.g., Chantrell *et al* 1978), in particular if particle clusters are present. First results of Eggemann *et al* (2007) show a strong influence of clustering on SLP. They found for well dispersed primary 10 nm particles a rarely measurable SLP while for clusters of similar particles much larger values were measured. There, a trivial effect is that the magnetic objects move from the superparamagnetic range towards the pseudo-single-domain range (cf figure 3), forming clusters similar to those shown in figure 2(b). However, magnetic structure within these clusters is unknown so far. Strong indications for particle interactions were also found by Shcherbakov and Fabian (2005) while analysing the temperature dependence of ac susceptibility and remanence in natural tuff as well as ferrofluid samples.

Further potential for increasing SLP doubtless exists if besides magnetic iron oxides other magnetic particles are taken into consideration, too. In relaxation theory, the maximum SLP is proportional to the dc susceptibility χ_0 (cf equations (7)), the main parameter of which is saturation magnetization of the particles. The validity was proved previously for maghemite particles (Hergt *et al* 2004a, 2004b, Glöckl *et al* 2006). For Co nanoparticles ($M_s = 700$ kA m^{-1}), first SLP measurements revealed an extreme value of 770 W g^{-1} at 400 kHz and 10 kA m^{-1} (Zeisberger *et al* 2007). Since for the particles used in these experiments mean core size and size distribution was not yet optimized with respect to SLP, further enhancement seems to be achievable. Moreover, one of the highest saturation magnetizations of 2 MA/m is shown by Fe_3Co (see, e.g., Hütten *et al* 2005). This is a factor of five times the magnetization of maghemite. Consequently, the potential SLP of these particles may be expected to be of the order of 10 kW g^{-1}.

Acknowledgments

The authors thank Professor Wilfried Andrä for valuable discussions. They are indebted to Dr Norbert Buske for providing the magnetic nanoparticles shown in figure 2(a). Thanks are due to Professor U Kaiser (figure 2(c)) and Dr Ch Oestreich (figure 2(b)) for transmission electron microscopy as well as Mrs Ch Schmidt for atomic force microscopy and XRD of magnetic nanoparticles.

References

Aharoni A 1996 *Introduction to the Theory of Ferromagnetism* (Oxford: Clarendon)

Aharoni A 1997 *Coherent and Incoherent Magnetization Processes in Non-interacting Particles in Magnetic Hysteresis in Novel Magnetic Materials* ed G C Hadjipanayis (Dordrecht: Kluwer–Academic)

Bertotti G 1998 *Hysteresis in Magnetism* (London: Academic)

Brezovich I A 1988 Low frequency hyperthermia *Med. Phys. Monogr.* **16** 82–111

Butler R F and Banerjee S K 1975 Theoretical single-domain grain size range in magnetite and titanomagnetite *J. Geophys. Res.* **80** 4049–58

Chantrell R W, Popplewell J and Charles S W 1978 Measurements of particle size distribution parameters in ferrofluids *IEEE Trans. Magn.* **14** 975–7

Debye P 1929 *Polar Molecules* (New York: Dover)

Dunin-Borkowski R E, McCartney M R, Pósfai M, Frankel R B, Bazylinski D A and Buseck P R 2001 Off-axis electron holography of magnetotactic bacteria: magnetic microstructure of strains MV-1 and MS-1 *Eur. J. Mineral.* **13** 671–84

Dutz S, Andrä W, Hergt R, Müller R, Oestreich Ch, Schmidt Ch, Töpfer J, Zeisberger M and Bellemann M 2007a Influence of dextran coating on the magnetic behavior of iron oxide nanoparticles *J. Magn. Magn. Mater.* **311** 51–4

Dutz S, Buske N, Hergt R, Müller R, Zeisberger M, Görnert P and Röder M 2005 Preparation of water based dispersions of magnetic iron oxide nanoparticles in the mean diameter range of 15–30 nm *Proc. 6th German Ferrofluid-Workshop* p 50

Dutz S, Clement J, Eberbeck D, Gelbrich T, Hergt R, Müller R, Wotschadlo J and Zeisberger M 2008 Ferrofluids of magnetic multicore nanoparticles for biomedical applications *J. Magn. Magn. Mater.* submitted

Dutz S, Hergt R, Mürbe J, Müller R, Zeisberger M, Andrä W, Töpfer J and Bellemann M E 2007b Hysteresis losses of magnetic nanoparticle powders in the single domain size range *J. Magn. Magn. Mater.* **308** 305–12

Eagle D F and Mallinson J C 1967 On the coercivity of γ-Fe_2O_3 particles *J. Appl. Phys.* **38** 995–7

Eggemann A S, Majetich S A, Farrell D and Pankhurst Q A 2007 Size and concentration effects on high frequency hysteresis of iron oxide nanoparticles *IEEE Trans. Magn.* **43** 2451–3

Fabian K, Kirchner A, Williams W, Heider F, Leibl F and Hubert A 1996 Three-dimensional micromagnetic calculations for magnetite using FFT *Geophys. J. Int.* **124** 89–104

Glöckl G, Hergt R, Zeisberger M, Dutz S, Nagel S and Weitschies W 2006 Effect of field parameters, nanoparticle properties and immobilization on the specific heating power in magnetic particle hyperthermia *J. Phys.: Condens. Matter* **18** 2935–49

Gneveckow U, Jordan A, Scholz R, Bruss V, Waldöfner N, Ricke J, Feussner A, Hildebrandt B, Rau B and Wust P 2004 Description and characterization of the novel hyperthermia- and thermoablation system *Med. Phys.* **31** 1444–51

Gneveckow U, Jordan A, Scholz R, Eckelt L, Maier-Hauff K, Johannsen M and Wust P 2005 Magnetic force nanotherapy *Biomed. Tech.* **50** 92–3

Heider F, Dunlop D J and Sugiura N 1987 Magnetic properties of hydrothermally recrystallized magnetite crystals *Science* **236** 1287–90

Hergt R and Andrä W 2007 Magnetic Hyperthermia and Thermoablation *Magnetism in Medicine* 2nd edn, ed W Andrä and H Nowak (Berlin: Wiley–VCH)

Hergt R, Andrä W, d'Ambly C G, Hilger I, Kaiser W A, Richter U and Schmidt H G 1998 Physical limits of hyperthermia using magnetite fine particles *IEEE Trans. Magn.* **34** 3745–54

Hergt R and Dutz S 2007 Magnetic particle hyperthermia—biophysical limitations of a visionary tumour therapy *J. Magn. Magn. Mater.* **311** 187–92

Hergt R, Dutz S, Müller R and Zeisberger M 2006 Magnetic particle hyperthermia: nanoparticle magnetism and materials development for cancer therapy. *J. Phys.: Condens. Matter* **18** 2919–34

Hergt R, Hiergeist R, Hilger I and Kaiser W A 2002 Magnetic nanoparticles for thermoablation *Recent Res. Dev. Mat. Sci.* **3** 723–42

Hergt R, Hiergeist R, Hilger I, Kaiser W A, Lapatnikov Y, Margel S and Richter U 2004a Maghemite nanoparticles with very high AC-losses for application in RF-magnetic hyperthermia *J. Magn. Magn. Mater.* **270** 345–57

Hergt R, Hiergeist R, Zeisberger M, Glöckl G, Weitschies W, Ramirez L P, Hilger I and Kaiser W A 2004b Enhancement of AC-losses of magnetic nanoparticles for heating applications *J. Magn. Magn. Mater.* **280** 358–68

Hergt R, Hiergeist R, Zeisberger M, Schüler D, Heyen U, Hilger I and Kaiser W A 2005 Magnetic properties of bacterial magnetosomes as potential diagnostic and therapeutic tools *J. Magn. Magn. Mater.* **293** 80–6

Heyen U and Schüler D 2003 Growth and magnetosome formation by microaerophilic magnetospirillum strains in an oxygen-controlled fermentor *Appl. Microbiol. Biotechnol.* **61** 536–44

Hilger I, Hergt R and Kaiser W A 2005 Use of magnetic nanoparticle heating in the treatment of breast cancer *IEE. Proc. Nanobiotechnol.* **152** 33–9

Hubert A and Schäfer R 1998 *Magnetic Domains* (Berlin: Springer)

Hütten A, Sudfeld D, Ennen I, Reiss G, Wojczykowski K and Jutzi P 2005 Feromagnetic FeCo nanoparticles for biotechnology *J. Magn. Magn. Mater.* **293** 93–101

Johannsen M, Gneveckow U, Thiesen B, Taymoorian K, Chie H C, Waldöfner N, Scholz R, Jordan A, Loening S A and Wust P 2007 Thermotherapy of prostate cancer using magnetic nanoparticles *Eur. Urol.* **52** 1653–62

Klokkenburg M, Vonk C, Claesson E M, Meeldijk J D, Erné B H and Philipse A P 2004 Direct imaging of zero-field dipolar structures in colloidal dispersions of synthetic magnetite *J. Am. Chem. Soc.* **126** 16706–7

Kneller E 1966 Theorie der magnetisierungskurve kleiner kristalle *Encyclopedia of Physics* (*Ferromagnetism* vol XVIII/2) ed H P J Wijn (Berlin: Springer) pp 438–544

Kneller E 1969 *Magnetism Metallurgy* vol 1, ed A E Berkovitz and E Kneller (New York: Academic) pp 365–471, chapter VIII (Fine Particle Theory) (English version)

Kronmüller H and Fähnle M 2003 *Micromagnetism and the Microstructure of Ferromagnetic Solids* (Cambridge: Cambridge University Press)

Kurland H-D, Grabow J, Staupendahl G, Andrä W, Dutz S and Bellemann M E 2007 Magnetic iron oxide nanopowders produced by CO_2 laser evaporation *J. Magn. Magn. Mater.* **311** 73–7

Landau L D and Lifshitz E M 1960 *Electrodynamics of Continuos Media* (London: Pergamon)

Mee C D and Daniel E D 1996 *Magnetic Recording Technology* (New York: McGraw-Hill)

Moroz P, Jones S K and Gray B N 2002 Magnetically mediated hyperthermia: current status and future directions *Int. J. Hyperthermia* **18** 267–84

Müller R, Hergt R, Dutz S, Zeisberger M and Gawalek W 2006 Nanocrystalline iron oxide and Ba-ferrite particles in the transition range superparamagnetism-ferromagnetism for ferrofluid applications *J. Phys.: Condens. Matter* **18** 2527–42

Néel L 1949 Influence des fluctuations thermiques a l'aimantation des particules ferromagnétiques *CR Acad. Sci.* **228** 664–8

Rosensweig R E 2002 Heating magnetic fluid with alternating magnetic field *J. Magn. Magn. Mater.* **252** 370–4

Shcherbakov V P and Fabian K 2005 On the determination of magnetic grain-size distributions of superparamagnetic particle ensembles using the frequency dependence of susceptibility at different temperatures *Geophys. J. Int.* **162** 736–46

Siegenthaler U 1994 *Klinische Pathophysiologie* (Stuttgart: Thieme-Verlag)

Stoner E C and Wohlfarth E P 1948 A mechanism of magnetic hysteresis in heterogeneous alloys *Phil. Trans. R. Soc.* A **240** 599–642

Sun S and Zeng H 2002 Size controlled synthesis of magnetite nanoparticles *J. Am. Chem. Soc.* **124** 8204–5

Tartaj P, del Puerto-Morales M, Veintemillas-Verdaguer S, Gonzalez-Carreno T and Serna C J 2003 The preparation of magnetic nanoparticles for applications in biomedicine *J. Phys. D: Appl. Phys.* **36** R182–97

Witt A, Fabian K and Bleil U 2005 Three-dimensional micromagnetic calculations for naturally shaped magnetite: Octahedra and magnetosomes *Earth Planet. Sci. Lett.* **233** 311–24

Zeisberger M, Dutz S, Müller R, Hergt R, Matoussevitch N and Bönnemann H 2007 Metallic cobalt nanoparticles for heating applications *J. Magn. Magn. Mater.* **311** 224–7